The secreted redox sensor roGFP2-Orp1 reveals oxidative dynamics in the plant apoplast

Julian Ingelfinger[1], Lisa Zander[2], Patricia L. Seitz[3], Oliver Trentmann[1], Sophie Tiedemann[3]; Stefanie Sprunck[3], Thomas Dresselhaus[3], Andreas J. Meyer[2], Stefanie J. Müller-Schüssele[1]

[1] Molecular Botany, Department of Biology, RPTU Kaiserslautern-Landau, D-67633 Kaiserslautern, Germany

[2] Chemical Signalling, Institute of Crop Science and Resource Conservation (INRES), University of Bonn, D-53113 Bonn, Germany

[3] Cell Biology and Plant Biochemistry, Institute of Plant Sciences, University of Regensburg, D-93053 Regensburg, Germany

ORCIDs: 0000-0002-4434-4193 (J.I.); 0009-0009-0681-6311 (P.L.S.); 0000-0002-9530-5848 (OT); 0000-0002-9732-9237 (S.S.); 0000-0001-6442-4302 (T.D.); 0000-0001-8144-4364 (A.J.M.); 0000-0003-4061-1175 (S.J.M.-S.)

Correspondence:

Stefanie Müller-Schüssele

RPTU Kaiserslautern-Landau

Erwin-Schrödinger-Str. 70

67663 Kaiserslautern

mueschue@rptu.de

Tel.: +49 (0)631-205-4391

Fax: +49 (0)631-205-2998

Keywords: *Arabidopsis thaliana*, *Physcomitrium patens*, redox-sensitive GFP, oxidative burst, genetically encoded biosensor, apoplast, ROS

Abstract

Specific generation of reactive oxygen species (ROS) is important for signalling and defence in many organisms. In plants, different types of ROS perform useful biological functions in the extracellular space (apoplast) supporting processes such as polymerisation and cell wall remodelling. In addition, increased formation of extracellular superoxide and hydrogen peroxide occurs during immune responses. Our current knowledge of apoplastic ROS dynamics is based on luminescence assays, ROS staining methods and indirect evidence via changes to intracellular redox balance. However, dynamic monitoring of extracellular redox processes *in vivo* remains difficult.

Using two evolutionary distant land plant model species, the moss *Physcomitrium patens* and the flowering plant *Arabidopsis thaliana*, we test whether the genetically encoded redox biosensor roGFP-Orp1 can be used to assess extracellular redox dynamics. We found that secreted roGFP-Orp1 can inform about local diffusion barriers, as well as protein cysteinyl oxidation rate in the apoplast after pre-reduction. Observed re-oxidation rates were surprisingly slow within the range of hours. Comparing *A. thaliana* to *P. patens*, we found faster sensor re-oxidation that increased after triggering an immune response. Our data indicate differences in extracellular oxidative processes between species and within a species, depending on immune signalling.

INTRODUCTION

Most intracellular compartments, such as the cytosol, plastids and mitochondria constitute a reducing environment for protein cysteinyl groups, as they contain glutathione (GSH) in the mM range, as well as a glutathione reductase that keeps this pool reduced, transferring electrons from NADPH (Marty *et al.*, 2009, 2019). In contrast, the extracellular space of plants is characterised by low concentrations of glutathione (less than 1% of total GSH), resulting from GSH or glutathione disulfide (GSSG) export (Ohkama-Ohtsu *et al.*, 2007; Zechmann, 2014). GSSG is enzymatically degraded in the apoplast (Ohkama-Ohtsu *et al.*, 2007; Noctor *et al.*, 2012). Importantly, no thiol-reducing systems are known for the apoplast (Meyer *et al.*, 2021). Oxidative protein folding in the secretory pathway prepares proteins for this oxidising environment, ensuring correct formation of disulfides. Measurements of glutathione redox potential (E_{GSH}) in the ER-lumen using redox-sensitive GFPs (roGFP) revealed an E_{GSH} of less negative than -241 mV (Birk *et al.*, 2013; Ugalde *et al.*, 2022*a*).

Although the apoplast seems to be a ‘one-way-street’ in terms of thiol redox biology, redox processes in the apoplast have been implicated in growth, development and reproduction as well as signalling and immunity. To foster cell growth, metabolites constituting building blocks for extracellular polymers, such as the cuticle and cell wall components, are exported (Renault

et al., 2017). Polymer formation or loosening is induced *in situ*, involving oxidative processes mediated by different ROS types, such as superoxide ($O_2^{\cdot-}$), hydrogen peroxide (H_2O_2) and hydroxyl radical formation (Liszkay *et al.*, 2004; Tenhaken, 2015; Cosgrove, 2022). Here, class III peroxidases responding with different catalytic cycles to the local hydrogen peroxide (H_2O_2)/superoxide ($O_2^{\cdot-}$) balance can mediate formation of hydroxyl radicals that cause cell wall loosening (Chen and Schopfer, 1999; Tenhaken, 2015). Development- and immunity-related cell wall signalling is partially overlapping, often involving membrane-spanning receptor-like kinases (Wolf, 2022). Extracellular $O_2^{\cdot-}$ and H_2O_2 are further involved in evolutionary conserved stress-induced long-distance signalling (Miller *et al.*, 2009; Fichman *et al.*, 2023; Koselski *et al.*, 2023) as well as immune responses. Signal amplification involves specific formation of $O_2^{\cdot-}$ via transmembrane Respiratory Burst Oxidase Homologs (RBOHs) transferring electrons from cytosolic NADPH to extracellular oxygen, triggering a cascade of extracellular ROS formation (Mhamdi and Van Breusegem, 2018; Waszczak *et al.*, 2018; Sies *et al.*, 2022). After generation, $O_2^{\cdot-}$ dismutates via enzymatic catalysis or spontaneously (in low pH) to the more stable ROS H_2O_2 (and O_2). Oxidative burst signalling and RBOH function in immunity are evolutionary conserved in land plants (Lehtonen *et al.*, 2012; Bressendorff *et al.*, 2016; Chu *et al.*, 2023).

Moreover, extracellular and intracellular redox dynamics can be linked (Mittler *et al.*, 2022). Thus, extracellular ROS balance influences the plasma membrane proteome and nanodomain formation (Martinière *et al.*, 2019). A first transmembrane redox-responsive receptor kinase (HPCA1) involved in long distance signaling has been described (Castro *et al.*, 2021). Changes of intracellular H_2O_2 levels mediated via peroxiporins and/or diffusion has been evidenced using genetically encoded biosensors (Nietzel *et al.*, 2019; Ugalde *et al.*, 2022*b*; Arnaud *et al.*, 2023) and investigated using *in vitro* reconstitution of cytosolic redox-active proteins (Vogelsang *et al.*, 2024). Here, biosensors with high sensitivity to H_2O_2-dependent oxidation, such as HyPer (Pak *et al.*, 2020) and roGFP2-Orp1 (Gutscher *et al.*, 2009; Nietzel *et al.*, 2019) were employed successfully to monitor compartment-specific changes in redox states over extended time periods (Nietzel *et al.*, 2019; Niemeyer *et al.*, 2021; Ugalde *et al.*, 2021; Arnaud *et al.*, 2023; Dopp *et al.*, 2023; Vogelsang *et al.*, 2024). Fluorescence read-out of roGFP2 offers high robustness to pH changes, as the protonated chromophore still emits fluorescence, in contrast to many other fluorescent proteins (Schwarzländer *et al.*, 2008; Müller-Schüssele *et al.*, 2021). Redox-responsiveness of roGFP2 is mediated by an GSH/GRX-dependent thiol switch on the outer face of the GFP β-barrel structure (Hanson *et al.*, 2004; Meyer and Dick, 2010) (**Fig. 1A**). Oxidation rates of roGFP2 can be coupled to H_2O_2 levels via proteins containing peroxidatic cysteines, such as yeast Orp1 (Oxidant receptor peroxidase 1, (Ma *et al.*, 2007)). This type of protein-based redox sensor is oxidised by H_2O_2 and reduced via GSH (Gutscher *et al.*, 2009; Nietzel *et al.*, 2019) (**Fig. 1A**) and can be expressed in a model

organism and compartment of choice. In summary, specific local changes in extracellular ROS levels are involved in immunity, signalling and extracellular polymer formation or loosening. It is however unclear how dynamic extracellular protein cysteinyl redox states can be and what oxidation rates are reached *in vivo* in different species. Mechanisms affecting cysteine thiol steady state oxidation levels in the apoplast await identification. Staining procedures for different ROS types support changes in ROS levels but often cannot resolve temporal or compartmentalised dynamics. Here, we investigate whether secreted roGFP2-Orp1 can be used to sense apoplastic redox dynamics, using two evolutionary distant land plant model species with different body plans and alternation of generations, the moss *Physcomitrium patens* and the flowering plant *Arabidopsis thaliana*.

MATERIAL AND METHODS

Plant material and growth conditions

Physcomitrium patens (Hedw.) Bruch & Schimp ecotype 'Gransden 2004' (International Moss Stock Centre (IMSC, http://www.moss-stock-center.org), accession number 40001) was grown axenically and regularly sub-cultured in liquid medium (Knop medium: 250 mg l^{-1} KH_2PO_4, 250 mg l^{-1} KCl, 250 mg l^{-1} $MgSO_4 \times 7\ H_2O$,1 g l^{-1} Ca $(NO_3)_2 \times 4\ H_2O$ and 12.5 mg l^{-1} $FeSO_4 \times 7\ H_2O$, pH 5.8) (Reski and Abel, 1985) supplemented with micro-elements (ME), (H_3BO_3, $MnSO_4$, $ZnSO_4$, KI, $Na_2MoO_4 \times 2\ H_2O$, $CuSO_4$, $Co(NO_3)_2$) (Egener *et al.*, 2002). For experimental analyses, *P. patens* gametophores were grown on Knop ME agar plates (12 g l^{-1} purified agar; Oxoid, Thermo Scientific). Light intensity in growth cabinets was set to 70-100 µmol photons m^{-2} s^{-1} and 16:8 h light/dark cycle at 23°C. To induce gametangia development, plates with four weeks old colonies were transferred into a growth cabinet which was set to c. 30 µmol photons m^{-2} s^{-1} and 8:16 h light/dark cycle at 15°C for at least two weeks. *Arabidopsis thaliana* ecotype Columbia 0 (Col-*0*) was used as wild-type (WT) background. Seeds were sown directly on potted soil (ED73 (Patzer Erden, Germany) with 17.6 % (v/v) sand) and stratified in the dark for 48 h at 4°C. Afterwards they were transferred to a plant growth chamber (Fitotron SGC2, Weiss Technik) with light intensity set to c. 130 µmol photons m^{-2} s^{-1} and 8:16 h light/dark cycle at 23°C. After two weeks seedlings were separated with fine forceps, so that only one seedling per pot remained. Four to six weeks after separation the plants were used for experiments.

N. benthamiana seeds were germinated in soil in a pot and grown at 22 °C, 16:8 h light/dark and 250 µmol m^{-2} s^{-1} light intensity. Two-week-old seedlings were transplanted into individual pots and used to infiltrate *Agrobacteria* into leaves at around 4-6 weeks of age.

Cloning and transient transformation

Both constructs for secreted roGFP2-Orp1 were generated using the GATEWAY™ cloning technology (Invitrogen; Thermo Fisher Scientific). For *P. patens*, the endogenous aspartic protease 1 signal peptide ($AP1_{sp}$, M1-R28 of Pp3c5_19520V3.1) (Schaaf *et al.*, 2004) and for *A. thaliana* the endogenous chitinase signal peptide ($CHI_{sp,}$ M1-A23 of AT3G12500.1) (Haseloff *et al.*, 1997; Meyer *et al.*, 2007; Ugalde *et al.*, 2022*a*) were amplified using PCR (Phusion™ High Fidelity DNA Polymerase, Thermo Fisher Scientific): The $AP1_{sp}$ was amplified, adding an *attB1* site and an overlap to roGFP2 using the primer B1_AP1sp_F GGGGACAAGTTTGTACAAAAAAGCAGGCTTAatgggggcatcgaggagt and AP1sp_ro2Orp_P2 GCCCTTGCTCACCATgcgagggcttgcctcagc. RoGFP2-Orp1 was amplified, adding an *attB2* site and overlap to the $AP1_{sp}$ with the primer AP1sp_ro2Orp_P3 gaggcaagccctcgcATGGTGAGCAAGGGCGAG and B2_ro2_R: GGGGACCACTTTGTACAAGAAAGCTGGGTCTATTCCACCTCTTTCAAAAGTTCT. The fragments were fused in an overlap PCR using the primer B1_AP1sp_F and B2_ro2_R. The resulting $AP1_{sp}$-roGFP2-Orp1 fragment was cloned into *pDONR207* via BP reaction (BP Clonase™II Enzyme Mix, Thermo Fisher Scientific). After sequencing, a positive clone was used for LR reaction (LR Clonase™II Enzyme Mix, Thermo Fisher Scientific) into *PTA2Act5GW* (Bohle *et al.*, 2024*b*), creating a plant expression construct under the control of the *P. patens Actin 5* promoter (Weise *et al.*, 2006).

In accordance, the CHI_{sp} was amplified, adding an *attB1* site and an overlap to roGFP2 using the following primer B1_CHIsp_F: GGGGACAAGTTTGTACAAAAAAGCAGGCTTAatgaagactaatctttttctctttc and CHIsp_ro2_P2 CTCGCCCTTGCTCACggcgaattcggccgagga. RoGFP2-Orp1 was amplified, adding an *attB2* site and overlap to the CHI_{sp}, using the primer P3_CHIsp_ro2_F: tcggccgaattcgccGTGAGCAAGGGCGAGGAG and B2_ro2(Orp1)_R: GGGGACCACTTTGTACAAGAAAGCTGGGTCTATTCCACCTCTTTCAAAAGTTCT. The two fragments were combined in an overlap PCR using the B1_CHIsp_F and B2_ ro2(Orp1)_R primer. The fragment was cloned into *pDONR207* via BP reaction, generating *pENTR207L1L2-CHIsp-roGFP2-Orp1*. After sequencing, a positive clone was used for LR reaction into *pSS02* (derivative of pMDC32 (Curtis and Grossniklaus, 2003)) via LR reaction, creating a plant expression construct under the control of the *A. thaliana Ubiquitin10* promoter. For transient expression in *N. benthamiana* epidermal leaf cells, the binary expression vector *$35S_{pro}$:CHIsp-roGFP2-Orp1* was cloned by Gibson assembly. The *CHIsp-roGFP2-Orp1* fragment was amplified from *pENTR207L1L2-CHIsp-roGFP2-Orp1* using the primer pair CHIsp_roGFP2_linker_Orp1(F: caatttactattctagtcgaATGAAGACTAATCTTTTTCTCTTTC and R: tgcggactctagcatggccgCTATTCCACCTCTTTCAAAAG). The vector fragment was amplified from the destination vector *pH2GW7* (Karimi *et al.*, 2002) with the primer pair pH2GW7 F:

CGGCCATGCTAGAGTCCG and R: TCGACTAGAATAGTAAATTGTAATGTTGTTTGTTG. Both fragments were amplified using KOD Xtreme™ Hot Start DNA Polymerase and ligated via Gibson assembly using NEBuilder® HiFi DNA Assembly Master Mix according to manufacturer's instructions. Gateway™ LR Clonase™ II was employed to create the binary expression vector *35S$_{pro}$:tagRFPt-RemA* (plasma membrane marker) by recombining the ENTRY vector *pENTR_tagRFPt-RemA* (Cyprys *et al.*, 2019), which contains tagRFPt N-terminally fused to the membrane anchor of *M. truncatula* SYMREM1 (Konrad *et al.*, 2014), with the destination vector *pB2GW7* (Karimi *et al.*, 2002). Both expression vectors were transformed into chemically competent *Agrobacterium* strain GV3101 (pMP90RK). Single colonies were picked and grown for 48 h in liquid YEP medium (10 g l^{-1} yeast extract, 10 g l^{-1} peptone, and 5 g l^{-1} NaCl) containing the corresponding antibiotics and cultured to OD_{600} = 0.8 before resuspension in infiltration buffer (5 % (w/v) sucrose, 0,01 % Silwet L-77, 450 µM acetosyringone, few crumbs of $MgSO_4$ and glucose). The cultures were mixed at 1:1 ratio and co-infiltrated into *N. benthamiana* leaves as described previously for *N. tabacum* (Sparkes *et al.*, 2006). After 48 h, plasmolysis was induced by injecting 1 M sorbitol into the infiltrated leave areas and incubation for 15-30 min before microscopic analysis.

Generation of transgenic lines

Stable transgenic *P. patens* lines were generated using polyethylene-glycol mediated protoplast transformation, as described in Hohe *et al.* (2004). For transformation, purified *PTA2Act5GW-AP1sp-roGFP2-Orp1* plasmid was cut near *PTA2* homologous regions (Kubo *et al.*, 2013) using *BglII* and *NotI* and mixed in a molar ratio of c. 2:1 with the uncut resistance plasmid *pBsNNNEV*, containing the *nptII* neomycin resistance gene under the control of a *NOS* promoter and terminator. Plants surviving four weeks on selection (Knop ME with 12.5 µg ml^{-1} G418) were transferred to Knop ME and screened for sensor fluorescence after growth for c. 2 weeks.

Transformation of *A. thaliana* was performed by the floral dip method (Clough and Bent, 1998). Briefly, competent *AGL-1 Agrobacterium tumefaciens* cells were transformed with an error-free expression clone of *pSS02-CHIsp-roGFP2-Orp1* using electroporation and selected on agar containing Rifampicin, Ampicillin and Kanamycin (all 50 µg ml^{-1}). For floral dip, an overnight culture of a positive *A. tumefaciens* colony was inoculated and after reaching an OD_{600} of approximately 0.8, the cells were harvested by centrifugation for 10 minutes at 5000 g. The supernatant was discarded, and the pellet resuspended in 400 ml dipping solution (5% sucrose, 0.02% Silwet Gold). *A. thaliana* plants containing flower buds were dipped twice with a time interval of 6-7 days. T1-transformants were selected on ½ MS (Murashige & Skoog + Vitamins 0.22%, Duchefa), 0.1% sucrose, 0.8% agar plates, pH 5.7, containing 20 µg ml^{-1} Hygromycin B (Duchefa). After germination, seedlings with long hypocotyls, longer roots as wells as green cotyledons were transferred to soil. T1 plants were screened for fluorescence

and presence of a single T-DNA was confirmed using segregation analysis of T2 seedlings. Experiments shown were conducted with material from homozygous T4 and T5 plants.

Microscopic imaging of roGFP2-Orp1

For ratiometric analysis, confocal laser scanning microscopy of roGFP2-Orp1 in the apoplast of *P. patens* leaflets and *A. thaliana* leaf discs was realised on a LSM880 (Axio Observer.Z1, Carl Zeiss, Oberkochen, Germany) using a x40 (C-Apochromat x40/1.2 W) objective by exciting roGFP2 sequentially at 405 nm (diode laser, 1/0.5 % (*A. thaliana* / *P. patens*)) and 488 nm (argon laser, 1/3.5 % (*A. thaliana* / *P. patens*)) and detecting roGFP2 emission between 509 nm and 535 nm. Autofluorescence was detected at 425-470 nm after excitation at 405 nm. Chlorophyll autofluorescence was detected at 680-735 nm after excitation at 488 nm. For roGFP2-Orp1 calibration, *P. patens* gametophores and *A. thaliana* leaf discs were submerged in imaging buffer (10 mM MES, 5 mM KCl, 10 mM $CaCl_2$, 10 mM $MgCl_2$ pH 5.8 (Wagner *et al.*, 2019)) or imaging buffer supplemented with either 5 mM 2,2'-dipyridyl disulfide (DPS) or 10 mM dithiothreitol (DTT) and incubated until complete oxidation or reduction, which was reached within 30 min to 1 h. Fluorescence ratio calculations and further image analysis was performed in a MATLAB-based ratio software (RRA) (Fricker, 2016). For plasmolysis, 600 mM Mannitol was used for *A. thaliana* and 600 mM NaCl was used for *P. patens*. The degree of oxidation (OxD) of roGFP2 was calculated according to Schwarzländer *et al.* (2008).

Transiently transformed *Nicotiana benthamiana* leaves were imaged, using a Visitron VisiScope spinning disc microscope with a Leica DMi8 body, a Yokogawa CSU-W1 spinning disc unit, a Visitron sCMOS pco.edge camera and a 40x/1.2 water immersion objective. The 488 nm laser was used for excitation of GFP, tagRFP was excited with the 561 nm laser. Images were processed using Fiji (Schindelin *et al.*, 2012).

Overview images of fluorescence intensity were taken at a fluorescence stereomicroscope (Leica M205 FCA with Leica K3C camera, Plan Apo 0.63x and 2x corr. objective), using 405-40 ex./525-50 em. and 470-40 ex./525-50 em. filter combinations.

Plate reader-based read-out of roGFP2-Orp1 fluorescence

Ratiometric time-series measurements for roGFP2-Orp1 fluorescence were carried out using a CLARIOstar® Plus plate reader (BMG Labtech). The roGFP2 signal was detected using a sequential filter-based excitation of 400-10 nm and 482-16 nm, with the emission detected using a 530-40 nm filter, using top optics. For *P. patens* expressing $AP1_{sp}$-roGFP2-Orp1 whole gametophores were transferred to a 96 well plate (3-5 per well) and incubated in 200 µl imaging buffer (10 mM MES, 5 mM KCl, 10 mM $CaCl_2$, 10 mM $MgCl_2$ pH 5.8) overnight in the dark at room temperature. The next day, the imaging buffer was replaced and, after another hour in the dark, the measurement was started (Ugalde *et al.*, 2022*a*). After measuring the initial fluorescence of the untreated samples, the measurement was paused and the treatment was

added. In some experiments the measurement was paused again to remove and wash out the treatment 3 x 5 min with 200 µl imaging buffer, after observing complete sensor reduction.

For assays with *A. thaliana* expressing *CHI$_{sp}$-roGFP2-Orp1*, 7 mm leaf discs were punched out and floated on imaging buffer overnight in the dark with the adaxial side facing up. On the next day the leaf discs were transferred to a 96 well plate and pushed to the bottom of the well with the adaxial side facing down. After one hour of incubation in imaging buffer in the dark, the buffer was replaced and leaf discs used for fluorescence read-out of roGFP2-Orp1 as described above, but via bottom optics (Ugalde *et al.*, 2022*a*). To trigger oxidative bursts, a flagellin fragment (*flg22*, AS-62633, Eurogentec, Cologne, Germany) was used as elicitor and added manually to a final concentration of 1 µM in the respective wells.

Statistical analysis

Two-way ANOVA followed by Tukey's multiple comparisons test was performed using GraphPad Prism version 10.4.0 (or later versions) for Windows (GraphPad Software, Boston, Massachusetts USA, www.graphpad.com)**.**

RESULTS

Generation of stable plant lines secreting roGFP2-Orp1 to the apoplast

To obtain stable plant lines expressing and secreting roGFP2-Orp1 (**Fig. 1A**) to the apoplast, we added suitable signal peptides for targeting to the secretory pathway to the N-terminus of existing roGFP2-Orp1 constructs (Nietzel *et al.*, 2019). To this end, we employed the endogenous signal peptide of aspartic protease 1 (AP1sp) from *P. patens* (Schaaf *et al.*, 2004; Hoernstein *et al.*, 2018), as well as an endogenous chitinase signal peptide from *A. thaliana* (Haseloff *et al.*, 1997; Meyer *et al.*, 2007; Ugalde *et al.*, 2022*a*) (**Fig. 1B**). Correct protein targeting to the apoplast was confirmed by transient expression of *CHIsp-roGFP2-Orp1* together with a plasma membrane marker in *Nicotiana benthamiana* epidermal cells (**Fig. S1**). Subsequently, we stably transformed *P. patens* and *A. thaliana* and selected several independent fluorescent plant lines expressing secreted roGFP2-Orp1. No growth differences were observed for transgenic lines and two independent lines per species chosen for further analyses. By inducing plasmolysis, we confirmed the localisation of fluorescent signal in the apoplast for both species (**Fig. 1C, Fig. S2**). While roGFP2 fluorescence was evenly distributed in leaflets of moss gametophores (**Fig. 1C**, **Fig. S2**, **Fig. S3A, B**), it was mainly visible in perpendicular walls in filamentous moss protonema (**Fig. S3C**). In *A. thaliana*, roGFP2 fluorescence signal intensities differed between tissues: the strongest signals were observed in lobes of pavement cells in epidermis as well as hypocotyls of seedlings (**Fig. 1C, Fig. S3D, E, F**), whereas mesophyll cells showed a heterogenous signal distribution with punctuate signals at contact points between cells (**Fig. S3G**). Sensor fluorescence intensity in roots was lower, except for the root tip (**Fig. S3H, I**).

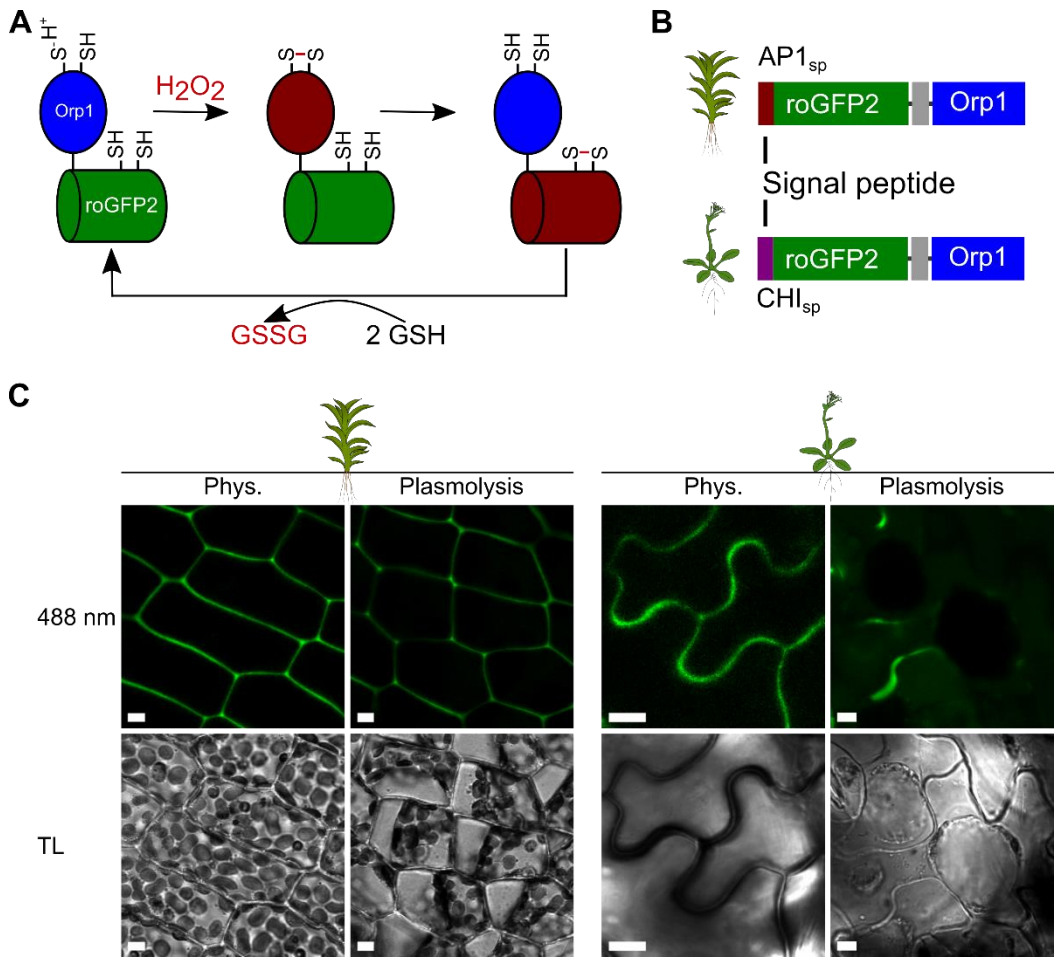

Figure 1: Creation of stable transgenic lines expressing secreted roGFP2-Orp1 in *P. patens* and *A. thaliana*
A Simplified scheme showing oxidation and reduction pathways for the redox biosensor roGFP2-Orp1. The reduced form of Orp1 is depicted in blue and for roGFP2 in green, the oxidised forms of both domains are depicted in red. **B** Construct design, adding a suitable signal peptide for secretion to the *roGFP2-linker-Orp1* coding sequence: CHI_{sp} for *A. thaliana* and $AP1_{sp}$ for *P. patens*. **C** Exemplary confocal images of *P. patens* leaflets (line #131) and *A. thaliana* pavement cells (line 3B) stably expressing *$AP1_{sp}$-roGFP2-Orp1* or *CHI_{sp}-roGFP2-Orp1*, respectively. Plasmolysis was induced using 0.6 M Mannitol (*A. thaliana*) or 0.6 M NaCl (*P. patens*). TL, transmitted light; scale bars = 5 µm.

Calibration of secreted roGFP2-Orp1

Next, we assessed the redox state of secreted roGFP2-Orp1 by ratiometric imaging and ratiometric plate reader-based fluorescence read-out for both species. To test functionality and dynamic range of secreted roGFP2-Orp1, we fully reduced and oxidised the sensor protein *in vivo*, using the reductant dithiothreitol (DTT) and the thiol-specific oxidant 2,2'-dipyridyl disulfide (DPS) (Lopez-Mirabal *et al.*, 2007). Using confocal microscopy and image analysis (Fricker, 2016; Ugalde *et al.*, 2022*a*), we found that roGFP2-Orp1 dynamic range (δ) was between c. 1.8 and 2.5 in moss leaflets (**Fig. 2A, B** individual channels shown in **Figs. S4**), while it was increased in the reproductive structures, the gametangia, to c. 3 to 4 (**Fig. S5, S6**).

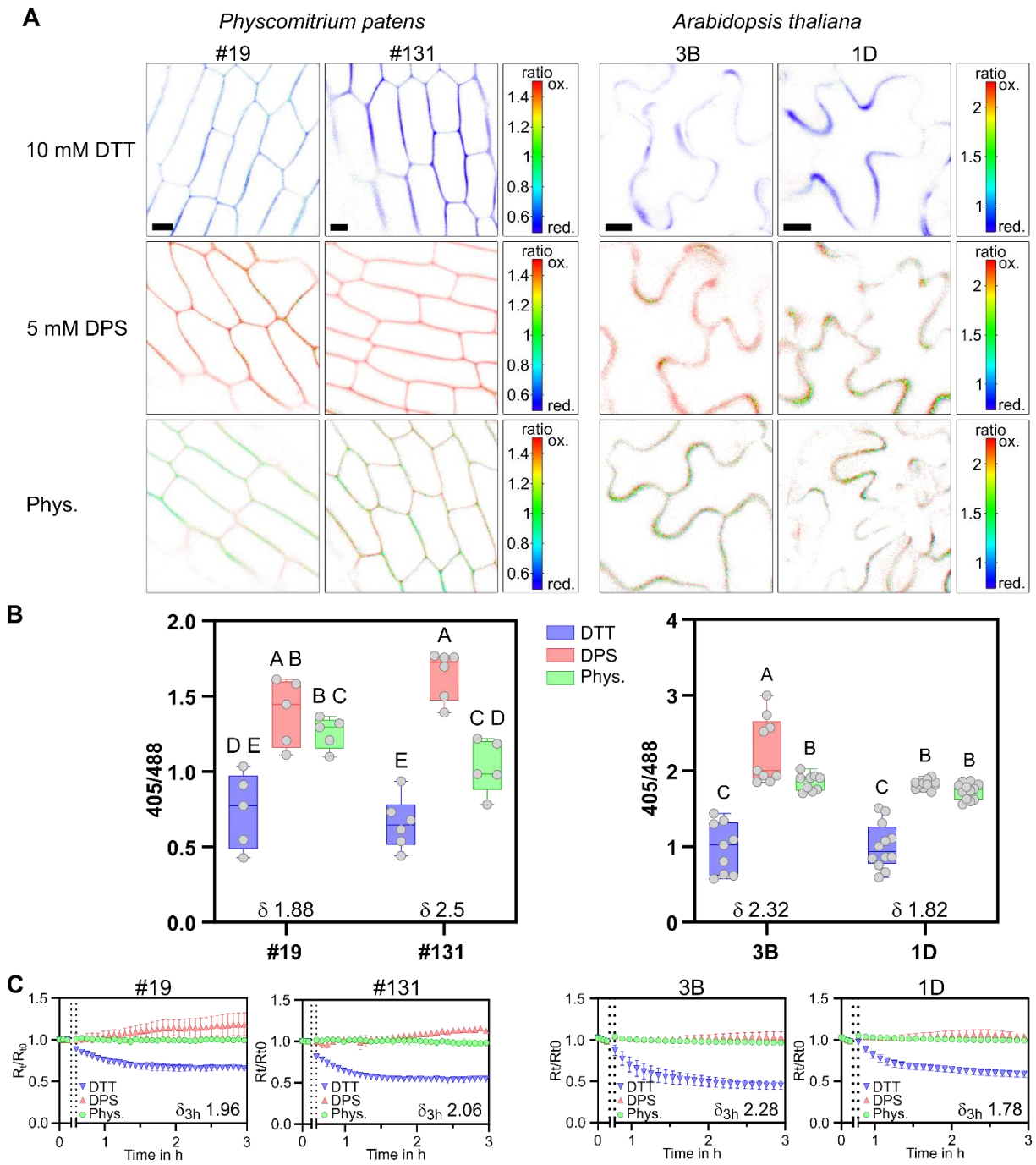

Figure 2: Calibration of apoplastic roGFP2-Orp1 in *P. patens* and *A. thaliana*
Calibration is shown for two independent lines of *P. patens* expressing *AP1$_{sp}$-roGFP2-Orp1* (left panels) and two independent lines of *A. thaliana* expressing *CHI$_{sp}$-roGFP2-Orp1* (right panels). 10 mM dithiothreitol (DTT) was used for full reduction and 5 mM 2,2'-dipyridyl disulfide (DPS) was used for full oxidation of the biosensor *in vivo*. **A** Sensor 405/488 redox ratio depicted as false-colour ratio scale in confocal microscopy images. Scale bars = 10 µm. **B** Box plots of redox ratio analysis using confocal microscopy images. The measured dynamic range is indicated by δ. Boxes show 25% to 75% quartiles, the line indicates the median, the whiskers show min and max, individual data points are shown as circles, n = 5-12. Different letters indicate significant differences according to a two-way ANOVA with Tukey's multiple comparison post-hoc test, $p < 0.05$. **C** *In vivo* calibration of roGFP2-Orp1 measured as a time series using leaf discs (*A. thaliana*) or gametophores (*P. patens*) in a multi-well plate reader. Graphs depict 400-10/482-16 ratios, normalised to the ratio mean before treatment (R_t/R_{t0}). Opening of the plate reader and start of the treatment is indicated by two dashed lines, n = 5.

We found a similar dynamic range of c. 1.8 to 2.3 in *A. thaliana* leaf epidermis and mesophyll (**Fig. 2A, B**; individual channels shown in **Fig. S7, S8**). Using plate reader-based fluorescence

read-out from gametophores and leaf discs (Wagner *et al.*, 2019; Ugalde *et al.*, 2022*a*), we measured a slightly smaller or similar dynamic range between c. 1.8 and 2.3 during sensor calibration over time in both species (**Fig. 2C**). As calibration was possible in all tested tissues, it is possible to determine the *in vivo* redox state of roGFP2-Orp1 by investigating non-treated, physiological samples (phys.). Both ratiometric measurement methods confirmed that roGFP2-Orp1 is mainly oxidised when secreted (data for physiological state without treatments in **Fig. 2A, B, C**), with many physiological values not significantly different from fully oxidised sensor controls. Based on the individual calibrations, we calculated mean degrees of sensor oxidation (OxD) in physiological state ranging from 65%+/-13% to 87%+/-5% for *P. patens* and 75% +/- 3% to 90% +/- 6% in *A. thaliana*, which is similar to the 96.5 % that was shown in Arnaud *et al.* (2023). Plate reader-based measurements, that integrate biosensor signal over a high number of cells suggested that secreted roGFP2-Orp1 was not completely oxidised *in vivo* in *P. patens*, as plateau mean values for physiological measurements were consistently lower than mean values for oxidised controls (**Fig. 2C**). Interestingly, using confocal microscopy some heterogeneity of sensor oxidation was visible both in *A. thaliana* and *P. patens*, especially in areas of high sensor signal.

Monitoring protein cysteinyl oxidation kinetics in the apoplast

While the oxidation rate of roGFP2-Orp1 is dependent on changes in H_2O_2 levels, reduction of the roGFP2 reporter domain is dependent on the GSH/GRX system intracellularly. In the apoplast, the sensor oxidation state could thus be potentially used as a read-out for changes in H_2O_2 levels, if the sensor disulfides can be pre-reduced. Thus, we tested different doses and types of thiol reducing agents, using the stable lines expressing secreted roGFP2-Orp1. To this end, we first used DTT, that already proofed successful in apoplastic sensor calibration (**Fig. 2**). After reaching plateau reduction levels, we subsequently removed DTT, washed the samples stringently and investigated sensor re-oxidation rates (**Fig. S9**). A direct comparison of *P. patens* and *A. thaliana*, including sensor calibration, revealed that secreted roGFP2-Orp1 oxidation rates after pre-reduction showed species-specific differences, with barely any re-oxidation observable for *P. patens* gametophores and re-oxidation in *A. thaliana* leaf discs within the range of hours (**Fig. S9**). To titrate exposure to the reducing agent DTT, we reduced DTT doses from 10 mM to 1 mM and found that 2.5 mM DTT was sufficient to fully reduce secreted roGFP2-Orp1 in approximately 2-4 h in both species (**Fig. S10**). Re-oxidation occurred only slowly in *A. thaliana* leaf discs in a period of c. 10 h and using 5 mM or more DTT led to incomplete sensor re-oxidation in the monitored time period of c. 20 h. Notably, re-oxidation in *P. patens* remained consistently low, independently of the used amount of DTT **(Fig. S9)**.

As DTT penetrates cells and as complete reduction of cells might cause reductive stress and disturb ER function (Ugalde *et al.*, 2022*a*), we next tested a reducing agent that is non-cell permeable. To this end, we used 5 mM TCEP (tris(2-carboxyethyl)phosphine) (Cline *et al.*, 2004). As a control, we tested TCEP effects using *A. thaliana* leaf discs expressing cytosolic roGFP2-Orp1 and found no effect during 4 h incubation (**Fig. S11**). Interestingly, cytosolic roGFP2-Orp1 showed a potential oxidation after removal of TCEP (**Fig. S11**). Incubating *A. thaliana* leaf discs with 5 mM TCEP led to complete reduction of secreted roGFP2-Orp1, while full dynamic range was not reached in *P. patens* gametophores (**Fig. 3A**). After washing out TCEP, secreted roGFP2-Orp1 re-oxidised in a range of c. 12 to 30 h in independent experiments in *A. thaliana*, while its redox state remained largely unchanged in *P. patens* gametophores. To test if roGFP2-Orp1 was still responsive to H_2O_2-mediated oxidation after pre-reduction, we added exogenous H_2O_2 after removal of reducing agent and observed rapid oxidation responses of secreted roGFP2-Orp1 *in vivo* in both species (**Fig. 3B**).

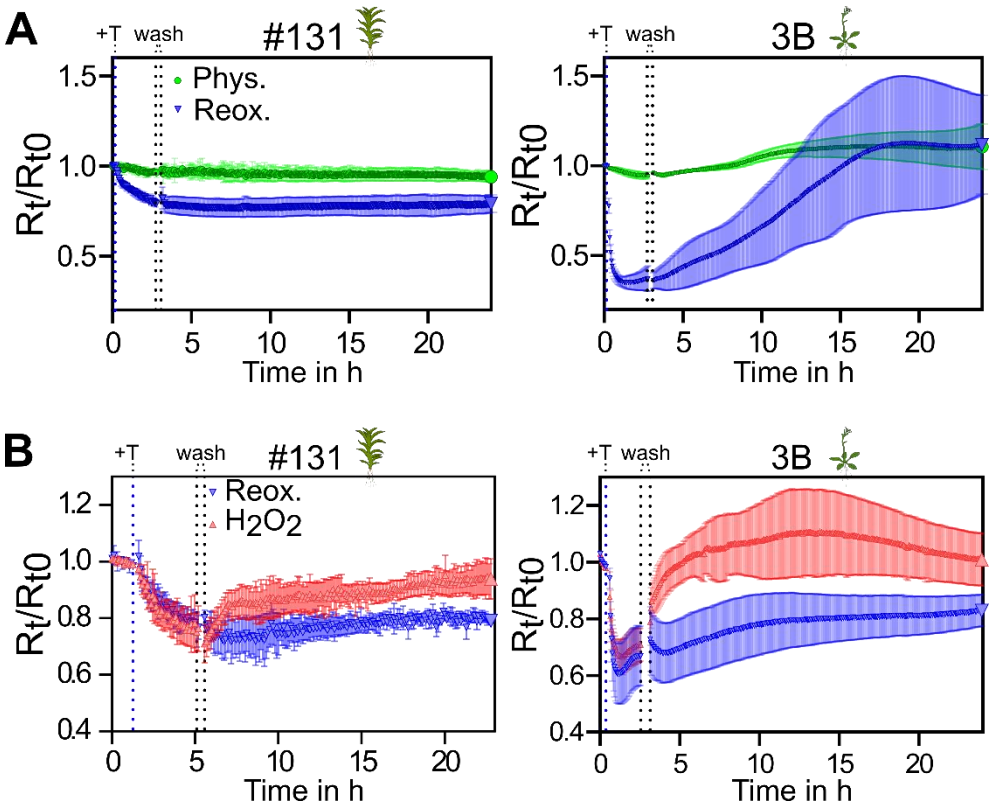

Figure 3: Re-oxidation rate of reduced apoplastic roGFP2-Orp1
Graphs depict 400-10/482-16 ratios, normalised to the ratio mean before treatment (R_t/R_{t0}), of apoplastic roGFP2-Orp1 measured as a time series using leaf discs (*A. thaliana*) or gametophores (*P. patens*) in a multi-well plate reader. Start of treatment with 5 mM TCEP is indicated by a blue dashed line (+T). After reaching plateau values the measurement was paused to remove and wash out the reducing agent, indicated by the two dashed lines (wash). **A** Comparison of apoplastic roGFP2-Orp1 re-oxidation rates in *P. patens* and *A. thaliana* after pre-reduction with 5 mM TCEP (blue inverted triangles), with untreated samples serving as physiological controls (phys., green circles), n = 5. **B** Comparison between inherent re-oxidation rate (blue inverted triangles) and re-oxidation by adding 10 mM H_2O_2 after washing (red triangle), n = 4 for *P. patens*, n = 5 for *A. thaliana*.

As re-oxidation rates of roGFP2-Orp1 were lower than expected *in vivo*, we investigated if activation of apoplastic $O_2^{\cdot-}$ production via RBOHs (Respiratory Burst Oxidase Homologs) would increase sensor oxidation rates. To this end, we used *A. thaliana* leaf discs and the peptide elicitor *flg22* (**Fig. 4**) (Felix *et al.*, 1999). Notably, addition of *flg22* leads to an increase in autofluorescence after excitation of fluorescence at 400 nm that was detectable in control leaf discs from WT without sensor expression (**Fig. 4A** grey overlay). This massive increase in autofluorescence interfered with fluorescence-based ratiometric roGFP2 read-out c. 5 h after addition of *flg22*. We thus restricted our analysis of the roGFP2-Orp1 400/480 fluorescence ratio the first 4 h after addition of *flg22*, that did not show an increase of autofluorescence in WT (**Fig. 4B**). In contrast to a control without addition of *flg22*, pre-reduced roGFP2-Orp1 re-oxidised during the first 3h after *flg22* addition, suggesting an increased H_2O_2-based oxidation rate in the apoplast. A second control sample, containing leaf discs expressing secreted roGFP2-Orp1 that were not pre-reduced showed a slight oxidative peak after addition of *flg22*, as well as the pre-reduced sample (grey diamonds in **Fig. 4B**). This transitory peak might be caused by the manual addition of *flg22*, and opening/closing of the plate reader, or represent a rapid transitory oxidation event, that is also affecting roGFP-Orp1 without pre-reduction. In summary, the elicitor-triggered immune response led to more rapid sensor re-oxidation in the apoplast of *A. thaliana* leaf discs, which was measurable via fluorescence read-out of roGFP2 in the first hours after initiation of an oxidative burst.

DISCUSSION

Observed heterogeneity of roGFP2-Orp1 levels and redox states. In this study we generated and characterised stable transgenic plant lines secreting the redox sensor roGFP2-Orp1, using the model bryophyte *P. patens* and the model flowering plant *A. thaliana*. Bryophytes are the sister clade to vascular plants, undergoing separate evolution since c. 480 Mio. years (Lang *et al.*, 2010; Donoghue *et al.*, 2021). Mosses display a dominant gametophytic generation, with juvenile tip-growing filamentous protonema and leafy gametophores (Kofuji and Hasebe, 2014; Müller *et al.*, 2016; Falz and Müller-Schüssele, 2019). By using species-specific signal peptides, we were able to mediate complete secretion of roGFP2-Orp1 in both model species, enabling further specific studies of sensor levels and redox steady state in the apoplast. We found that sensor levels differed between tissues for both species. In *P. patens*, protonema displayed lower roGFP2-Orp1 levels, with the highest fluorescence at perpendicular walls. This may be due to diffusion of secreted roGFP2-Orp1 into the surrounding media through protonema cell walls. This property of protonema is already known and used for biotechnological applications to secrete protein biopharmaceuticals into the surrounding media for downstream processing (Reski *et al.*, 2015). In contrast, roGFP2-Orp1 homogenously labelled the apoplastic space in gametophore leaflets, that possess a

cuticle (Renault *et al.*, 2017). Here, either cell wall density or the cuticle might limit the diffusion of secreted soluble particles out of the tissue. The *PpActin5* promoter was also active in moss gametangia, showing partially heterogenous signal with zones of high secretion and/or low diffusion.

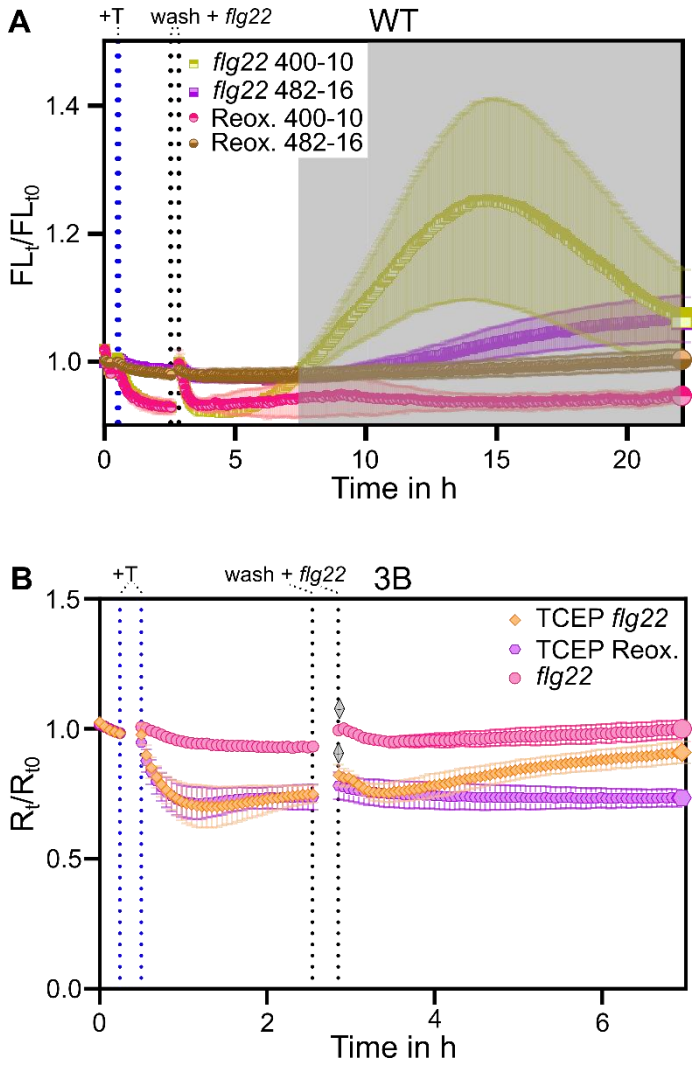

Figure 4: Re-oxidation of apoplastic roGFP2-Orp1 after triggering a *flg22*-induced oxidative burst
The fluorescence of *A. thaliana* leaf discs expressing CHI_{sp}-roGFP2-Orp1 and Col-*0* leaf discs was measured using a multi-well plate reader. The blue dashed lines indicate the addition of 5 mM TCEP. The black dashed lines indicate removal of TCEP and washing of samples. 1 µM *flg22* was added into the respective samples immediately before re-starting fluorescence measurements. **A** Autofluorescence control: Graph shows fluorescence intensity of Col-*0* control samples without sensor expression, normalised over the initial intensity before treatment, plotted over time, using same channel settings as in B; roGFP2 fluorescence channels are shown as separate lines, data from the same sample are indicated by mirrored symbols. Treatments: reduction and re-oxidation (Reox.), reduction and treatment with 1 µM *flg22* after washing (*flg22*), n = 3. **B** 400-10/482-16 ratio, normalised to the ratio mean before treatment (Rt/Rt0) of *A. thaliana* (line 3B), plotted over time. Treatments: No pre-reduction with TCEP (pink circle), pre-reduction with TCEP but no treatment with 1 µM *flg22* after washing (violet), pre-reduction with TCEP and treatment with 1 µM *flg22* after washing (orange), n = 5.

In comparison to *P. patens*, we observed higher heterogeneity of roGFP2-Orp1 fluorescence levels in *A. thaliana*. We currently interpret the higher fluorescence signals in lobes of pavement cells as well as in the meristematic/transition zone in root tips as indications of high secretion rates and/or low apoplastic diffusion rates. Punctate signals in mesophyll correlated

with contact points between cells in spongy mesophyll, also suggesting high secretion or low apoplastic protein diffusion for these zones.

Ratiometric analysis of roGFP2-Orp1 fluorescence in its physiological state revealed mostly oxidised sensor protein, as expected and previously tested for the extracellular environment (Arnaud *et al.*, 2023). The thiol-switch on roGFP2 has a consensus midpoint potential of -280 mV (pH7), that allows for sensitive measurement of redox changes in +/- 35 mV of this value (Müller-Schüssele *et al.*, 2021*b*). Thus, roGFP2 should be fully oxidised in the extracellular space with an estimated E_{GSH} less negative than -240 mV. Yeast Orp1 contains a peroxidatic cysteine (pK_a of 5.1 (Ma *et al.*, 2007)) that, via its thiolate state, attacks H_2O_2, leading to sulfenylation and subsequent disulfide formation. This disulfide is then transferred by a dithiol/disulfide exchange mechanism to the fused roGFP2 moiety (Gutscher *et al.*, 2009). Apoplastic pH in plants can rapidly change and has been measured as 6.3 in *A. thaliana* using the secreted pHluorin fluorescent sensor protein, with other values in literature ranging from c. 5 to 7 and potential spatio-temporal changes of up to 2 pH units (Gao *et al.*, 2004; Martinière *et al.*, 2013). Using fluorescent protein-based ‘Acidin’ biosensors, freely diffusing apoplastic sensor indicated a pH of c. 4.5 and showed very similar localisation pattern in lobes of pavement cells, compared to secreted roGFP2-Orp1 in this study (Moreau *et al.*, 2022). In low pH (below c. 5) fluorescence after excitation at 488 nm (B-band) will be quenched in GFP variants (containing S65T) (Elsliger *et al.*, 1999; Hanson *et al.*, 2004). In contrast, absorption after excitation at 405 nm (A-band) is increased in lower pH (Elsliger *et al.*, 1999), which will result in fluorescence in the case of roGFP2 (Hanson *et al.*, 2004). In consequence, roGFP2 oxidation state can be measured in the pH range expected, in comparison to the respective *in vivo* calibration. We were able to calibrate apoplastic roGFP2-Orp1 using thiol-specific reductants. The dynamic measurement range (δ) in our hands was smaller than the δ6.1 reached with purified sensor or δ6.5 of cytosol and δ4.1 mitochondria-targeted sensor *in vivo* (Nietzel *et al.*, 2019). It is already known that roGFP2-Orp1 δ decreases in lower pH (Nietzel *et al.*, 2019). Lower δ can additionally be caused by low signal-to-noise ratios, non-optimal settings, difficulties in administering reduction and oxidation agents for *in vivo* calibration and/or interfering autofluorescence in different tissues.

Assessing physiological redox states of secreted roGFP2-Orp1 by both confocal microscopy as well as plate reader-based fluorescence read-out suggested that a minor fraction of sensor molecules might exist in reduced state, especially in zones of high sensor signals. This finding needs to be interpreted cautiously, as there are several possible explanations for our observations. Expressing a thiol-containing sensor such as roGFP2-Orp1 under a high-level constitutive promoter might disturb ER redox homeostasis, causing reductive stress (Ugalde *et al.*, 2022*a*), resulting in secretion of proteins with reduced thiols. Alternatively, there might be spatio-temporal zonation in the apoplast, creating areas where the redox steady state of

protein cysteinyl groups (with similar characteristics to the protein sensor) is not completely oxidised. Mechanistically, possible reduction mechanisms affecting thiols in the apoplast are unclear to date, while both H_2O_2 and/or GSSG would mediate disulfide formation with slow rates non-enzymatically (Deponte, 2017).

What can we learn from secreted roGFP2-Orp1 regarding apoplastic redox dynamics?

To investigate oxidation rates for protein cysteinyl residues *in vivo*, we pre-reduced samples and monitored sensor re-oxidation rates. Notably, after reduction with either a cell-permeable or a non-cell-permeable reducing agent for thiols, roGFP2-Orp1 redox state was stable for c. 20 hours of monitoring in *P. patens* gametophores, and only slowly re-oxidised in the time frame of hours in leaf discs of *A. thaliana* (**Fig. 3**, **Fig. S9**). In contrast, re-oxidation after exogenous addition of H_2O_2 was fast, demonstrating responsiveness of roGFP2-Orp1. Without the presence of enzymatic catalysis via glutaredoxins (GRX), equilibration of proteins cysteinyl residue redox steady state and local E_{GSH} is slow (Gutscher *et al.*, 2008; Deponte, 2017; Bohle *et al.*, 2024*b*). Thus, E_{GSH}-dependent roGFP2 oxidation rates would potentially fit the observed sensor behaviour in the apoplast. In contrast, H_2O_2-mediated oxidation of Orp1 is kinetically fast, due to higher rate constants, even in the pH range expected for the apoplast. Thus, slow sensor re-oxidation indicates low H_2O_2-mediated oxidation rates in the apoplast under physiological conditions. Exact local H_2O_2 levels cannot be directly derived from sensor read-out, but roGFP2-Orp1 has been shown to sense as low as 0.1 µM H_2O_2 *in vitro* (Gutscher *et al.*, 2009; Nietzel *et al.*, 2019). According to current knowledge, RBOH activity causes a rapid extracellular increase of H_2O_2 levels. RBOHs are transmembrane proteins that can transfer electrons from cytosolic NADPH to extracellular oxygen, generating $O_2^{\cdot-}$ anions and in consequence H_2O_2 and O_2 by (spontaneous) dismutation. Extracellular H_2O_2 is implicated in multiple processes, including signalling and pathogen defence. As it is known that treatment with the bacterial elicitor *flg22* in *A. thaliana* leads to RBOHD-dependent apoplastic oxidative bursts within seconds to minutes (Miller *et al.*, 2009; Nietzel *et al.*, 2019), we investigated the effect of *flg22*-treatment on secreted roGFP2-Orp1 re-oxidation rates. As autofluorescence can rapidly increase in consequence to plant immune responses (Bohle *et al.*, 2024*a*), roGFP2 fluorescence-based read-out, especially after excitation in the UV range (e.g. 405 nm) needs to be carefully interpreted. Thus, the increase in autofluorescence bleed-through into the 400ex./520em. roGFP2 channel that we observed prohibits conclusions regarding the redox state after more than c. 4 hours after *flg22* treatment. However, we found increasing oxidation rates for pre-reduced roGFP2-Orp1 in the first hours after triggering RBOH activity via *flg22*. Compared to exogenous addition of 10 mM H_2O_2, re-oxidation rates after triggering an oxidative burst were slower. Using secreted roGFP-Orp1, we observed a minor transitory oxidation peak after *flg22* addition, which may be an artefact due to the manual addition of *flg22*. However, we observed a time lag of c. 1 h until apoplastic roGFP-Orp1 started oxidising

at a stable rate. Based on the known phases of ROS generation during an immune response (Ngou *et al.*, 2021; Arnaud *et al.*, 2023), an immediate increase in apoplastic H_2O_2 levels was expected. This raises the question why protein-based H_2O_2 sensing in the apoplast differs from luminol-based assays. Importantly, also intracellular redox biosensing revealed a time lag between luminol-based oxidative burst detection and intracellular oxidative changes (Nietzel et al., 2019; Ugalde et al., 2022b; Arnaud et al., 2023). Intracellular oxidation of cytosolic roGFP-Orp1 starts in the range of minutes to an hour after triggering an oxidative burst with *flg22* in *A. thaliana*, while H_2O_2-detection with luminol-based assays indicates a rapid peak in the first 20 min (Nietzel *et al.*, 2019; Arnaud *et al.*, 2023). Arnaud *et al.* (2023) revealed that the bi-phasic cytosolic roGFP2-Orp1 oxidation observed in response to *flg22*-triggered immune signalling was largely unchanged in *rbohd* plants. Thus, luminescence assays clearly evidence RBOHD activity, but RBOHD activity is not necessary for intracellular oxidation dynamics in response to *flg22*. In this context, our results suggest that extracellular oxidative changes occurring downstream of RBOH activity are not as massive as suggested by luminol-based assays, or more specific.

In conclusion, we found lower than expected oxidation rates for extracellular protein cysteinyl residues in *A. thaliana* that are even lower to absent in the model bryophyte *P. patens*. Our work provides first indications to the timeline of increasing apoplastic H_2O_2 levels in consequence to activating an immune response, as directly measured with a protein-based redox sensor. However, it is unclear to date if cysteinyl oxidation rates in the extracellular space are biologically relevant. In animal cells, dynamic redox steady states in the extracellular space are linked to several processes such as proliferation, differentiation and cell death (Banerjee, 2012). In land plants, the RBOH gene family has expanded and diversified, playing important roles in immunity, but also during reproduction (Mhamdi and Van Breusegem, 2018). How RBOHs fulfil their specific and diverse roles in creating local and dynamic apoplastic redox environments requires further investigations. In absence of interfering autofluorescence roGFP2-based sensors may be used to investigate oxidation dynamics. This approach could be particularly interesting to resolve spatial differences in a tissue context. Detection of apoplastic redox dynamics by cysteine-based sensors remains challenging, due to the need of pre-reduction. In addition, secreted roGFP2-Orp1 (or other pH-stable fluorescent proteins) can provide valuable information regarding zones of secreted protein retention and diffusion barriers in different plant species and tissues.

Supplementary data

The following supplementary figures are available:

Fig. S1. Transient expression of *CHI_{sp}-roGFP2-Orp1* in pavement cells of *Nicotiana benthamiana* leaves.

Fig. S2. Creation of stable transgenic lines expressing secreted roGFP2-Orp1 in *P. patens* and *A. thaliana* (additional independent lines)

Fig. S3. Fluorescence signal distribution of apoplastic roGFP2-Orp1 in *P. patens* and *A. thaliana*

Fig. S4. Confocal images of $AP1_{sp}$-roGFP2-Orp1 calibration in *P. patens*

Fig. S5. Confocal images of $Ap1_{sp}$-roGFP2-Orp1 calibration in *P. patens* gametangia (line #131)

Fig. S6. Confocal images $Ap1_{sp}$-roGFP2-Orp1 calibration in *P. patens* gametangia (line #19)

Fig. S7. Confocal images CHI_{sp}-roGFP2-Orp1 calibration in *A. thaliana* leaf discs (line 3B)

Fig. S8. Confocal images of CHI_{sp}-roGFP2-Orp1 calibration in *A. thaliana* leaf discs (line 1D)

Fig. S9. Re-oxidation rate of apoplastic roGFP2-Orp1 pre-reduced using DTT

Fig. S10. Re-oxidation rate of apoplastic roGFP2-Orp1 in *P. patens* and *A. thaliana* using varying doses of DTT

Fig. S11. Treatment with TCEP does not influence cytosolic roGFP2-Orp1 redox state in *A. thaliana*

Acknowledgements

We thank Aurora Martin (Molecular Botany, RPTU), Alexa Brox and Maria Homagk (Chemical Signalling, INRES, University of Bonn) for technical assistance. We are grateful to Anna-Lena Falz, Cloé Gadoud, Emma Müller, Sadia Tamanna, Ralf Pennther-Hager and Dominik Stehr for experimental support. We thank Markus Schwarzländer for providing plasmids and plant lines for cytosolic roGFP2-Orp1 expression, as well as useful discussion.

Author Contributions

JI, OT and SJMS designed the research. JI, LZ, PLZ and ST performed experiments and analysed data. SJMS, OT, AJM, TD and SS supervised the research and provided resources. JI and SJMS wrote the manuscript with contributions from all authors. All authors approved the manuscript before submission.

Conflict of Interest

The authors declare that they have no conflicts of interest.

Funding

This work was supported by the DFG-funded Research Unit FOR 5098 ‘Innovation and Coevolution in Plant Sexual Reproduction’ (JI, ST, SS, TD, SJMS). SJMS is grateful for funding obtained from BioComp 3.0 ‘Dynamic Membrane Processes in Biological Systems’.

References

Arnaud D, Deeks MJ, Smirnoff N. 2023. Organelle-targeted biosensors reveal distinct oxidative events during pattern-triggered immune responses. Plant Physiology **191**, 2551–2569.

Banerjee R. 2012. Redox outside the Box: Linking Extracellular Redox Remodeling with Intracellular Redox Metabolism. Journal of Biological Chemistry **287**, 4397–4402.

Birk J, Meyer M, Aller I, Hansen HG, Odermatt A, Dick TP, Meyer AJ, Appenzeller-Herzog C. 2013. Endoplasmic reticulum: reduced and oxidized glutathione revisited. Journal of Cell Science **126**, 1604–1617.

Bohle F, Klaus A, Ingelfinger J, *et al.* 2024*a*. Contrasting cytosolic glutathione redox dynamics under abiotic and biotic stress in barley as revealed by the biosensor Grx1-roGFP2. Journal of Experimental Botany **75**, 2299-2312.

Bohle F, Rossi J, Tamanna SS, *et al.* 2024*b*. Chloroplasts lacking class I glutaredoxins are functional but show a delayed recovery of protein cysteinyl redox state after oxidative challenge. Redox Biology **69**, 103015.

Bressendorff S, Azevedo R, Kenchappa CS, Ponce de Leòn I, Olsen JV, Rasmussen MW, Erbs G, Newman M-A, Petersen M, Mundy J. 2016. An Innate Immunity Pathway in the Moss *Physcomitrella patens*. The Plant Cell **28**, 1328–1342.

Castro B, Citterico M, Kimura S, Stevens DM, Wrzaczek M, Coaker G. 2021. Stress-induced reactive oxygen species compartmentalization, perception and signalling. Nature Plants **7**, 403–412.

Chen S, Schopfer P. 1999. Hydroxyl-radical production in physiological reactions. European Journal of Biochemistry **260**, 726–735.

Chu J, Monte I, DeFalco TA, Köster P, Derbyshire P, Menke FLH, Zipfel C. 2023. Conservation of the PBL-RBOH immune module in land plants. Current Biology **33**, 1130-1137.e5.

Cline DJ, Redding SE, Brohawn SG, Psathas JN, Schneider JP, Thorpe C. 2004. New Water-Soluble Phosphines as Reductants of Peptide and Protein Disulfide Bonds: Reactivity and Membrane Permeability. Biochemistry **43**, 15195–15203.

Clough SJ, Bent AF. 1998. Floral dip: a simplified method for *Agrobacterium*-mediated transformation of *Arabidopsis thaliana*. The Plant Journal **16**, 735–743.

Cosgrove DJ. 2022. Building an extensible cell wall. Plant Physiology **189**, 1246–1277.

Curtis MD, Grossniklaus U. 2003. A Gateway Cloning Vector Set for High-Throughput Functional Analysis of Genes in Planta. Plant Physiology **133**, 462–469.

Cyprys P, Lindemeier M, Sprunck S. 2019. Gamete fusion is facilitated by two sperm cell-expressed DUF679 membrane proteins. Nature Plants **5**, 253–257.

Deponte M. 2017. The incomplete glutathione puzzle: Just guessing at numbers and figures? Antioxidants & Redox Signaling **27**, 1130–1161.

Donoghue PCJ, Harrison CJ, Paps J, Schneider H. 2021. The evolutionary emergence of land plants. Current Biology **31**, R1281–R1298.

Dopp IJ, Kalac K, Mackenzie SA. 2023. Hydrogen peroxide sensor HyPer7 illuminates tissue-specific plastid redox dynamics. Plant Physiology **193**, 217–228.

Egener T, Granado J, Guitton M-C, *et al.* 2002. High frequency of phenotypic deviations in *Physcomitrella patens* plants transformed with a gene-disruption library. BMC Plant Biology **2**, 6.

Elsliger M-A, Wachter RM, Hanson GT, Kallio K, Remington SJ. 1999. Structural and Spectral Response of Green Fluorescent Protein Variants to Changes in pH. Biochemistry **38**, 5296–5301.

Falz A-L, Müller-Schüssele SJ. 2019. Physcomitrella as a model system for plant cell biology and organelle-organelle communication. Current Opinion in Plant Biology **52**, 7–13.

Felix G, Duran J, Volko S, Boller T. 1999. Plants recognize bacteria through the most conserved domain of flagellin. Plant J **18**, 265–276.

Fichman Y, Rowland L, Oliver MJ, Mittler R. 2023. ROS are evolutionary conserved cell-to-cell stress signals. Proceedings of the National Academy of Sciences **120**, e2305496120.

Fricker MD. 2016. Quantitative redox imaging software. Antioxidants & Redox Signaling **24**, 752–762.

Gao D, Knight MR, Trewavas AJ, Sattelmacher B, Plieth C. 2004. Self-reporting Arabidopsis expressing pH and [Ca^{2+}] indicators unveil ion dynamics in the cytoplasm and in the apoplast under abiotic stress. Plant Physiology **134**, 898–908.

Gutscher M, Pauleau A-L, Marty L, Brach T, Wabnitz GH, Samstag Y, Meyer AJ, Dick TP. 2008. Real-time imaging of the intracellular glutathione redox potential. Nature Methods **5**, 553–559.

Gutscher M, Sobotta MC, Wabnitz GH, Ballikaya S, Meyer AJ, Samstag Y, Dick TP. 2009. Proximity-based protein thiol oxidation by H_2O_2-scavenging peroxidases. The Journal of Biological Chemistry **284**, 31532–31540.

Hanson GT, Aggeler R, Oglesbee D, Cannon M, Capaldi RA, Tsien RY, Remington SJ. 2004. Investigating mitochondrial redox potential with redox-sensitive green fluorescent protein indicators. Journal of Biological Chemistry **279**, 13044–13053.

Haseloff J, Siemering KR, Prasher DC, Hodge S. 1997. Removal of a cryptic intron and subcellular localization of green fluorescent protein are required to mark transgenic *Arabidopsis* plants brightly. Proceedings of the National Academy of Sciences **94**, 2122–2127.

Hoernstein SNW, Fode B, Wiedemann G, *et al.* 2018. Host Cell Proteome of *Physcomitrella patens* Harbors Proteases and Protease Inhibitors under Bioproduction Conditions. Journal of Proteome Research **17**, 3749–3760.

Hohe A, Egener T, Lucht JM, Holtorf H, Reinhard C, Schween G, Reski R. 2004. An improved and highly standardised transformation procedure allows efficient production of single and multiple targeted gene-knockouts in a moss, *Physcomitrella patens*. Current Genetics **44**, 339–347.

Karimi M, Inzè D, Depicker A. 2002. GATEWAY™ vectors for *Agrobacterium*-mediated plant transformation. Trends in Plant Science **7**, 193–195.

Kofuji R, Hasebe M. 2014. Eight types of stem cells in the life cycle of the moss *Physcomitrella patens*. Current Opinion in Plant Biology **17**, 13–21.

Konrad SSA, Popp C, Stratil TF, Jarsch IK, Thallmair V, Folgmann J, Marín M, Ott T. 2014. S-acylation anchors remorin proteins to the plasma membrane but does not primarily determine their localization in membrane microdomains. New Phytologist **203**, 758–769.

Koselski M, Hoernstein SNW, Wasko P, Reski R, Trebacz K. 2023. Long-Distance Electrical and Calcium Signals Evoked by Hydrogen Peroxide in Physcomitrella. Plant And Cell Physiology **64**, 880–892.

Kubo M, Imai A, Nishiyama T, Ishikawa M, Sato Y, Kurata T, Hiwatashi Y, Reski R, Hasebe M. 2013. System for Stable β-Estradiol-Inducible Gene Expression in the Moss *Physcomitrella patens*. PloS one **8**, e77356.

Lang D, Weiche B, Timmerhaus G, Richardt S, Riaño-Pachón DM, Corrêa LGG, Reski R, Mueller-Roeber B, Rensing SA. 2010. Genome-wide phylogenetic comparative analysis of plant transcriptional regulation: a timeline of loss, gain, expansion, and correlation with complexity. Genome Biology and Evolution **2**, 488–503.

Lehtonen MT, Akita M, Frank W, Reski R, Valkonen JPT. 2012. Involvement of a Class III Peroxidase and the Mitochondrial Protein TSPO in Oxidative Burst Upon Treatment of Moss Plants with a Fungal Elicitor. Molecular Plant-Microbe Interactions **25**, 363–371.

Liszkay A, Van Der Zalm E, Schopfer P. 2004. Production of Reactive Oxygen Intermediates ($O_2^{\bullet-}$, H_2O_2, and $^{\bullet}OH$) by Maize Roots and Their Role in Wall Loosening and Elongation Growth. Plant Physiology **136**, 3114–3123.

Lopez-Mirabal HR, Thorsen M, Kielland-Brandt MC, Toledano MB, Winther JR. 2007. Cytoplasmic glutathione redox status determines survival upon exposure to the thiol-oxidant 4,4′-dipyridyl disulfide. FEMS Yeast Research **7**, 391–403.

Ma L-H, Takanishi CL, Wood MJ. 2007. Molecular Mechanism of Oxidative Stress Perception by the Orp1 Protein. Journal of Biological Chemistry **282**, 31429–31436.

Martinière A, Desbrosses G, Sentenac Hervé, Paris N. 2013. Development and properties of genetically encoded pH sensors in plants. Frontiers in Plant Science **4**, 523.

Martinière A, Fiche JB, Smokvarska M, Mari S, Alcon C, Dumont X, Hematy K, Jaillais Y, Nollmann M, Maurel C. 2019. Osmotic Stress Activates Two Reactive Oxygen Species Pathways with Distinct Effects on Protein Nanodomains and Diffusion. Plant Physiology **179**, 1581–1593.

Marty L, Bausewein D, Müller C, *et al.* 2019. Arabidopsis glutathione reductase 2 is indispensable in plastids, while mitochondrial glutathione is safeguarded by additional reduction and transport systems. The New Phytologist **224**, 1569–1584.

Marty L, Siala W, Schwarzländer M, Fricker MD, Wirtz M, Sweetlove LJ, Meyer Y, Meyer AJ, Reichheld J-P, Hell R. 2009. The NADPH-dependent thioredoxin system constitutes a functional backup for cytosolic glutathione reductase in Arabidopsis. Proceedings of the National Academy of Sciences **106**, 9109–9114.

Meyer AJ, Brach T, Marty L, Kreye S, Rouhier N, Jacquot J-P, Hell R. 2007. Redox-sensitive GFP in *Arabidopsis thaliana* is a quantitative biosensor for the redox potential of the cellular glutathione redox buffer. The Plant Journal **52**, 973–986.

Meyer AJ, Dick TP. 2010. Fluorescent protein-based redox probes. Antioxidants & Redox Signaling **13**, 621–650.

Meyer AJ, Dreyer A, Ugalde JM, Feitosa-Araujo E, Dietz K-J, Schwarzländer M. 2021. Shifting paradigms and novel players in Cys-based redox regulation and ROS signaling in plants - and where to go next. Biological Chemistry **402**, 399–423.

Mhamdi A, Van Breusegem F. 2018. Reactive oxygen species in plant development. Development **145**, dev164376.

Miller G, Schlauch K, Tam R, Cortes D, Torres MA, Shulaev V, Dangl JL, Mittler R. 2009. The plant NADPH oxidase RBOHD mediates rapid systemic signaling in response to diverse stimuli. Science Signaling **2**, ra45-ra45.

Mittler R, Zandalinas SI, Fichman Y, Van Breusegem F. 2022. Reactive oxygen species signalling in plant stress responses. Nature Reviews Molecular Cell Biology **23**, 663–679.

Moreau H, Gaillard I, Paris N. 2022. Genetically encoded fluorescent sensors adapted to acidic pH highlight subdomains within the plant cell apoplast. Journal of Experimental Botany **73**, 6744–6757.

Müller SJ, Gütle DD, Jacquot J-P, Reski R. 2016. Can mosses serve as model organisms for forest research? Annals of Forest Science **73**, 135–146.

Müller-Schüssele SJ, Bohle F, Rossi J, Trost P, Meyer AJ, Zaffagnini M. 2021*a*. Plasticity in plastid redox networks: evolution of glutathione-dependent redox cascades and glutathionylation sites. BMC Plant Biology **21**, 322.

Müller-Schüssele SJ, Schwarzländer M, Meyer AJ. 2021*b*. Live monitoring of plant redox and energy physiology with genetically encoded biosensors. Plant Physiology **186**, 93–109.

Ngou BPM, Ahn H-K, Ding P, Jones JDG. 2021. Mutual potentiation of plant immunity by cell-surface and intracellular receptors. Nature **592**, 110–115.

Niemeyer J, Scheuring D, Oestreicher J, Morgan B, Schroda M. 2021. Real-time monitoring of subcellular H_2O_2 distribution in *Chlamydomonas reinhardtii*. The Plant Cell **33**, 2935–2949.

Nietzel T, Elsässer M, Ruberti C, *et al.* 2019. The fluorescent protein sensor roGFP2-Orp1 monitors in vivo H_2O_2 and thiol redox integration and elucidates intracellular H_2O_2 dynamics during elicitor-induced oxidative burst in Arabidopsis. The New Phytologist **221**, 1649–1664.

Noctor G, Mhamdi A, Chaouch S, Han Y, Neukermans J, Marquez-Garcia B, Queval G, Foyer CH. 2012. Glutathione in plants: an integrated overview: Glutathione status and functions. Plant, Cell & Environment **35**, 454–484.

Ohkama-Ohtsu N, Radwan S, Peterson A, Zhao P, Badr AF, Xiang C, Oliver DJ. 2007. Characterization of the extracellular *gamma*-glutamyl transpeptidases, GGT1 and GGT2, in Arabidopsis. The Plant Journal **49**, 865–877.

Pak VV, Ezeriņa D, Lyublinskaya OG, *et al.* 2020. Ultrasensitive genetically encoded indicator for hydrogen peroxide identifies roles for the oxidant in cell migration and mitochondrial function. Cell Metabolism **31**, 642-653.e6.

Renault H, Alber A, Horst NA, *et al.* 2017. A phenol-enriched cuticle is ancestral to lignin evolution in land plants. Nature Communications **8**, 14713.

Reski R, Abel WO. 1985. Induction of budding on chloronemata and caulonemata of the moss, *Physcomitrella patens*, using isopentenyladenine. Planta **165**, 354–358.

Reski R, Parsons J, Decker EL. 2015. Moss-made pharmaceuticals: from bench to bedside. Plant Biotechnology Journal. **13**, 1191-1198

Schaaf A, Reski R, Decker EL. 2004. A novel aspartic proteinase is targeted to the secretory pathway and to the vacuole in the moss *Physcomitrella patens*. European Journal of Cell Biology **83**, 145–152.

Schindelin J, Arganda-Carreras I, Frise E, *et al.* 2012. Fiji: an open-source platform for biological-image analysis. Nature Methods **9**, 676–682.

Schwarzländer M, Fricker MD, Müller C, Marty L, Brach T, Novak J, Sweetlove LJ, Hell R, Meyer AJ. 2008. Confocal imaging of glutathione redox potential in living plant cells. Journal of Microscopy **231**, 299–316.

Sies H, Belousov VV, Chandel NS, Davies MJ, Jones DP, Mann GE, Murphy MP, Yamamoto M, Winterbourn C. 2022. Defining roles of specific reactive oxygen species (ROS) in cell biology and physiology. Nature Reviews Molecular Cell Biology **23**, 499–515.

Sparkes IA, Runions J, Kearns A, Hawes C. 2006. Rapid, transient expression of fluorescent fusion proteins in tobacco plants and generation of stably transformed plants. Nature Protocols **1**, 2019–2025.

Tenhaken R. 2015. Cell wall remodeling under abiotic stress. Frontiers in Plant Science **5**, 771.

Ugalde JM, Aller I, Kudrjasova L, *et al.* 2022*a*. Endoplasmic reticulum oxidoreductin provides resilience against reductive stress and hypoxic conditions by mediating luminal redox dynamics. The Plant Cell **34**, 4007–4027.

Ugalde JM, Fecker L, Schwarzländer M, Müller-Schüssele SJ, Meyer AJ. 2022*b*. Live monitoring of ROS-induced cytosolic redox changes with roGFP2-based sensors in plants. In: Mhamdi A, ed. Methods in Molecular Biology. Reactive Oxygen Species in Plants. New York, NY: Springer US, 65–85.

Ugalde JM, Schlößer M, Dongois A, Martinière A, Meyer AJ. 2021. The latest HyPe(r) in plant H_2O_2 biosensing. Plant Physiology **187**, 480–484.

Vogelsang L, Eirich J, Finkemeier I, Dietz K-J. 2024. Specificity and dynamics of H_2O_2 detoxification by the cytosolic redox regulatory network as revealed by *in vitro* reconstitution. Redox Biology **72**, 103141.

Wagner S, Steinbeck J, Fuchs P, *et al.* 2019. Multiparametric real-time sensing of cytosolic physiology links hypoxia responses to mitochondrial electron transport. New Phytologist **224**, 1668–1684.

Waszczak C, Carmody M, Kangasjärvi J. 2018. Reactive oxygen species in plant signaling. Annual Review of Plant Biology **69**, 209–236.

Weise A, Rodriguez-Franco M, Timm B, Hermann M, Link S, Jost W, Gorr G. 2006. Use of *Physcomitrella patens* actin 5' regions for high transgene expression: importance of 5' introns. Applied Microbiology and Biotechnology **70**, 337–345.

Wolf S. 2022. Cell Wall Signaling in Plant Development and Defense. Annual Review of Plant Biology **73**, 323–353.

Zechmann B. 2014. Compartment-specific importance of glutathione during abiotic and biotic stress. Frontiers in Plant Science **5**, 566.